AGU PUBLICATIONS

Geophysical Research Letters

RESEARCH LETTER
10.1002/2015GL064861

Key Points:
- XBeach accurately reproduces the nearshore reef hydrodynamics at Roi-Namur
- Key parameters are fore reef slope, reef flat depth, width, and coral coverage
- Climate change will lead to increased coastal hazards on reef-lined islands

Supporting Information:
- Figures S1 and S2

Correspondence to:
C. Storlazzi,
cstorlazzi@usgs.gov

Citation:
Quataert, E., C. Storlazzi, A. van Rooijen, O. Cheriton, and A. van Dongeren (2015), The influence of coral reefs and climate change on wave-driven flooding of tropical coastlines, *Geophys. Res. Lett.*, *42*, 6407–6415, doi:10.1002/2015GL064861.

Received 8 JUN 2015
Accepted 5 JUL 2015
Accepted article online 7 JUL 2015
Published online 4 AUG 2015

The influence of coral reefs and climate change on wave-driven flooding of tropical coastlines

Ellen Quataert[1,2], Curt Storlazzi[3], Arnold van Rooijen[1], Olivia Cheriton[3], and Ap van Dongeren[1]

[1]Department of Applied Morphodynamics, Unit of Marine and Coastal Systems, Deltares, Delft, Netherlands, [2]Faculty of Civil Engineering and Geosciences, Delft University of Technology, Delft, Netherlands, [3]Pacific Coastal and Marine Science Center, U.S. Geological Survey, Santa Cruz, California, USA

Abstract A numerical model, XBeach, calibrated and validated on field data collected at Roi-Namur Island on Kwajalein Atoll in the Republic of Marshall Islands, was used to examine the effects of different coral reef characteristics on potential coastal hazards caused by wave-driven flooding and how these effects may be altered by projected climate change. The results presented herein suggest that coasts fronted by relatively narrow reefs with steep fore reef slopes (~1:10 and steeper) and deeper, smoother reef flats are expected to experience the highest wave runup. Wave runup increases for higher water levels (sea level rise), higher waves, and lower bed roughness (coral degradation), which are all expected effects of climate change. Rising sea levels and climate change will therefore have a significant negative impact on the ability of coral reefs to mitigate the effects of coastal hazards in the future.

1. Introduction

Coral reef platforms protect low-latitude coastal areas against hazards such as wave runup, overtopping, flooding, and erosion by dissipating wave energy some distance from the shoreline [*Ferrario et al.*, 2014]. However, wave-driven coastal flooding still occurs during extreme events such as tropical typhoons [*Péquignet et al.*, 2009; *Hoeke et al.*, 2013b]. Climate change-related sea level rise and changing wave conditions, as well as degrading reef properties, may have a negative impact on the protective capacities of coral reefs [*Storlazzi et al.*, 2011; *Grady et al.*, 2013; *Merrifield et al.*, 2014]. This may result in more frequent and extreme wave-driven coastal flooding events in the future.

The interaction between waves, ocean level, and the morphology of coral reefs leads to specific hydrodynamic processes. Transformation of waves in the 5–25 s incident band over reefs is characterized by strong wave energy dissipation, primarily due to wave breaking along the relatively steep fore reef [*Lee and Black*, 1978; *Young*, 1989; *Monismith et al.*, 2013] and bottom friction dissipation over the reef's rough bathymetry [*Lowe et al.*, 2005]. Wave breaking along the fore reef results in an increase of the mean water level on the reef flat due to wave-induced setup [*Gerritsen*, 1980; *Vetter et al.*, 2010; *Becker et al.*, 2014] and generates infragravity (IG) waves in the 25–1000 s band over the reef flat [*Symonds et al.*, 1982; *Péquignet et al.*, 2009; *Pomeroy et al.*, 2012; *Péquignet et al.*, 2014]. These processes, which can lead to large wave runup and flooding of the shore, are controlled by morphological parameters such as reef dimensions, topography, and roughness, as well as hydrodynamic forcing parameters such as offshore wave and tidal conditions. The objective of this paper is to use our field data and calibrated model to better understand how intrinsic reef properties such as morphology and climate change-induced effects on hydrodynamic forcing and roughness may affect coastal hazards along reef-lined coasts.

We used field data collected at Roi-Namur Island at the northern point of Kwajalein Atoll in the Republic of the Marshall Islands, where the reef morphology is representative for many atolls and fringing reef-lined coastlines. The data were used to calibrate a numerical model, which was then used to analyze the effect of variations in coral reefs and oceanographic forcing. In section 2, a description of the field site and a summary of the observed tidal and wave conditions are presented. The calibration and validation of the numerical model is presented in section 3. Using the model, the response of nearshore reef hydrodynamics to varying reef topography, water level, and wave conditions was investigated to provide insight into the effects of different coral reef characteristics and future trends in forcing on coastal hazards (section 4), followed by a discussion of how these may vary in the future due to climate change.

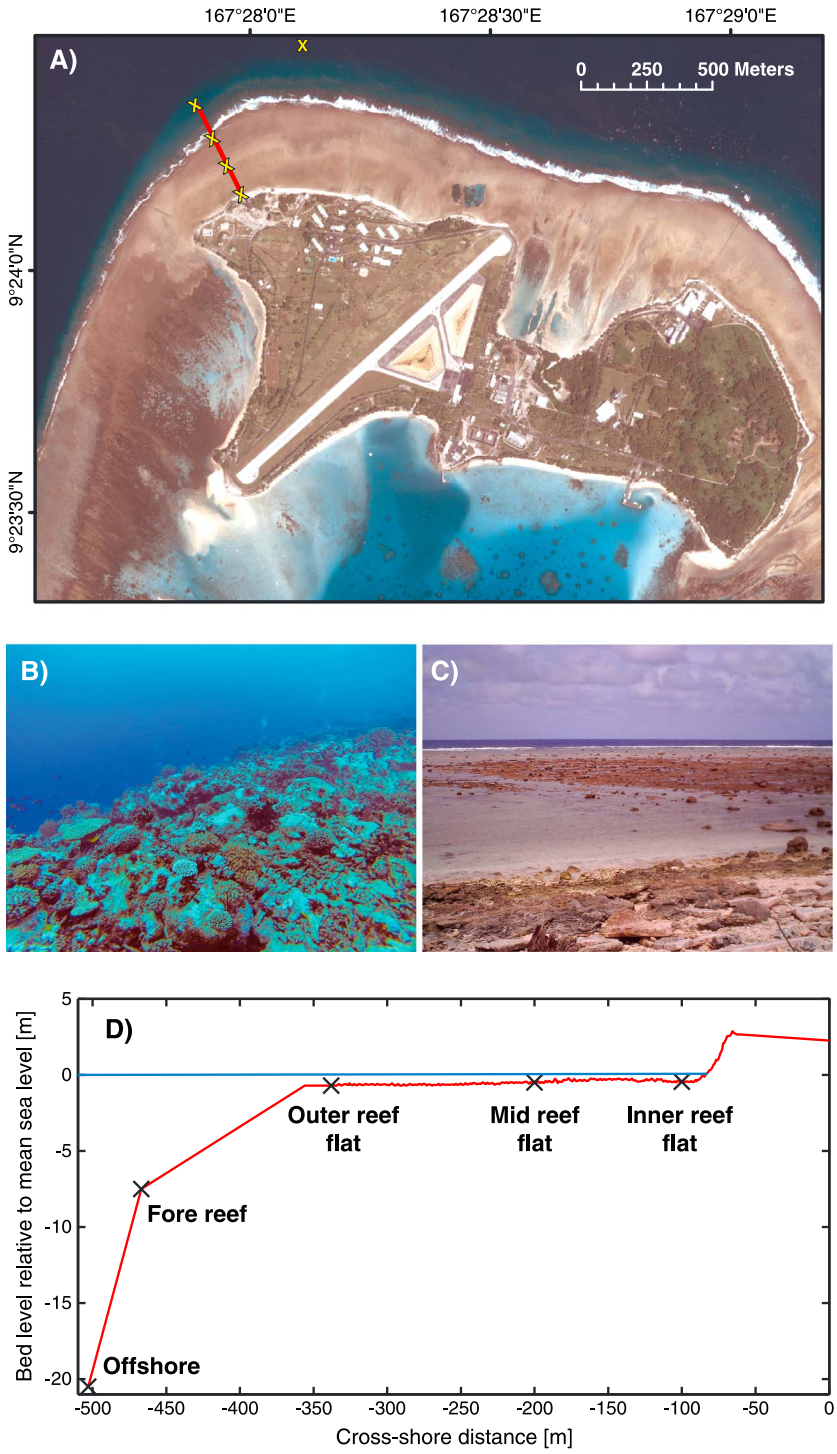

Figure 1. Views of the study: (a) location of the field site at Roi-Namur on Kwajalein Atoll; (b) fore reef topography; (c) reef flat topography visible at low tide; and (d) bathymetry along the cross-shore transect at Roi-Namur with the location of each pressure sensor (fore reef, outer, middle, and inner reef flat) and offshore AWAC.

2. Site Description and In Situ Observations

A field experiment was conducted from November 2013 to April 2014 along a cross-shore transect on Roi-Namur (Figure 1a). The fore reef has an approximately 1:20 slope and rough morphology covered by corals (Figure 1b). Between the fore reef and the island's shoreline is a relatively smooth (Figure 1c), very

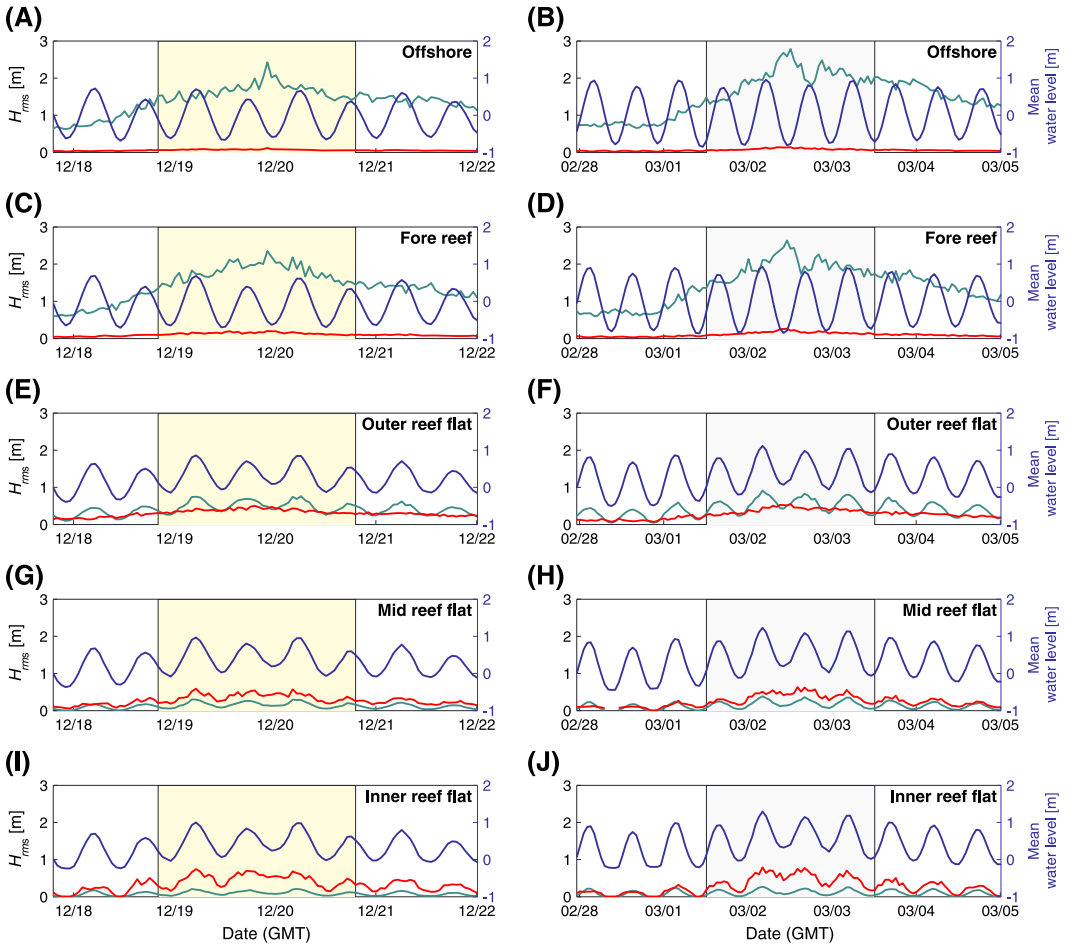

Figure 2. Roi-Namur reef hydrodynamics during the (a, c, e, g, and i) December 2013 event and (b, d, f, h, and j) March 2014 event. Burst-averaged mean water levels with respect to mean sea level (blue), and root-mean-squared wave heights for the infragravity wave band (red) and incident wave band (green). Yellow and grey areas indicate the periods used for (respectively) validation and calibration of the model.

gently sloping (~1:110) reef flat that is approximately 250 m wide and is almost fully exposed at low tide. The shoreline is characterized by a relatively steep beach (~1:6). The radius of curvature of the reef face is on the order of 650–700 m, which is much larger than typical incident wavelengths.

During the field experiment, an array of four bottom-mounted pressure sensors were deployed along the cross-shore transect. Pressure measurements were collected at 2 Hz for 34 min every hour. A Nortek Acoustic Wave and Current profiler (AWAC) was deployed at a depth of 21 m on the fore reef to provide deepwater wave conditions and recorded pressure measurements at 1 Hz for 34 min every hour. For consistency in methodology, pressure measurements from the AWAC were used instead of the dynamic acoustic surface tracking. Burst-averaged mean water levels were calculated from the pressure data. Surface elevation spectra provided significant wave heights (H_{m0}) and root-mean-squared wave heights (H_{rms}), based on infragravity wave (0.001–0.040 Hz) and incident wave bands (0.04–0.20 Hz).

The deployment period captured two highly energetic wave events (Figure 2) on 19 December 2013 ($H_{m0} = 3.4$ m; $T_p = 14$ s) and 2 March 2014 ($H_{m0} = 3.9$ m; $T_p = 14$ s), with near shore-normal incident wave directions of $3 \pm 8°$ (mean ± 1 standard deviation) from normal for the December event and $22 \pm 9°$ for the March event. These conditions resulted in extreme wave runup and flooding of the island. During these events, the wave height transformation over the reef toward the shore showed a general trend of decreasing incident wave height ($H_{rms,inc}$) and increasing infragravity wave height ($H_{rms,IG}$). A large amount of incident wave energy was dissipated between the fore reef and outer reef flat, primarily through wave breaking along the steep fore reef.

As a result, there was an increase in the mean water level on the reef flat due to the wave-induced setup. From the outer reef flat to the inner reef flat, $H_{rms,inc}$ continued to decrease due to frictional dissipation. Infragravity waves were generated in the incident wave breaking process [*Symonds et al.*, 1982; *Pomeroy et al.*, 2012], and their magnitudes increased toward the shoreline. This increase is in contrast with observations at the subaqueous Ningaloo reef in northwestern Australia by *Pomeroy et al.* [2012] and suggests that frictional dissipation plays a smaller role in the $H_{rms,IG}$ evolution at Roi-Namur due to the relatively smooth intertidal reef flat, similar to that observed off Guam [*Péquignet et al.*, 2014]. $H_{rms,IG}$ increased substantially and was dominant over $H_{rms,inc}$ near the shoreline. Furthermore, $H_{rms,inc}$ and $H_{rms,IG}$ on the reef flat were affected by the local reef flat tidal and wave setup-induced water depths [*Becker et al.*, 2014], primarily due to the effect of water depth variations on frictional dissipation rates.

3. Model Calibration and Validation

The XBeach model [*Roelvink et al.*, 2009] was used to simulate the hydrodynamics across the Roi-Namur reef. XBeach solves for water level variations up to the scale of long (infragravity) waves using the depth-averaged, nonlinear shallow water (NLSW) equations. The forcing is provided by a coupled wave action balance, in which the spatial and temporal variations of wave energy due to the incident-period wave groups are solved. The radiation stress gradients derived from these variations result in a wave force that is included in the NLSW equations and generates long waves and water level setup within the model. For a more extensive model description and formulations of XBeach (version 1.21.3667), reference is made to *Roelvink et al.* [2009].

Although the model was originally derived for mild-sloping sandy beaches, with some additional formulations, XBeach has been applied in reef environments [*Pomeroy et al.*, 2012; *Van Dongeren et al.*, 2013] and proved to accurately predict the key reef hydrodynamics. The additional formulations include the effect of higher bottom roughness on incident wave decay through the incident wave friction coefficient (f_w) and the current and infragravity wave friction coefficient (c_f), as outlined by *Van Dongeren et al.* [2013].

XBeach was applied in one-dimensional mode for the cross-shore transect of Roi-Namur using the measured transect bathymetry (Figure 1d). The application of a one-dimensional model neglects some of the dynamics that occur on natural reefs, such as lateral flow. However, it does represent a conservative estimate for infragravity generation and wave runup, as the forcing is shore normal. As stated above, the choice is warranted in this case because the observations show near-normally offshore waves. The model parameters f_w and c_f were calibrated for a 48 h simulation period during the March event (Figure 2), with all other model parameters, including the wave breaking parameters (discussed below) kept at default values. Next, the model was validated for the December event. For both calibration and validation, the measured burst-averaged offshore tidal elevations and wave conditions (Figure 2) were applied to the offshore boundary of the model domain. From the measured wave conditions (wave height, wave period, mean direction, and directional spreading), a sequence of hourly varying Joint North Sea Wave Project (JONSWAP) spectra were imposed following the approach of *Van Dongeren et al.* [2003].

Model results were assessed by comparing measured and modeled values of mean water levels, wave-induced setup (the local water level minus the offshore water level), $H_{rms,inc}$, and $H_{rms,IG}$ along the cross-shore profile (Figure 3). The predictive skill of the model was determined by calculating the bias and scatter index (SCI) as proposed by *Van der Westhuysen* [2010] for wave models. The best results were achieved with $f_w = 0.3$ and a spatially varying current friction coefficient, $c_{f,\text{fore reef}} = 0.1$ and $c_{f,\text{reef flat}} = 0.01$ on the sloping fore reef and reef flat, respectively. That these current friction coefficients differ between the fore reef and reef flat corresponds with the Roi-Namur reef topography (Figures 1b and 1c). These values are similar to those found by *Lowe et al.* [2005] and *Monismith et al.* [2013] for Kanaohe Bay (Hawaii) but smaller than those found for Ningaloo Reef (Western Australia), $f_w = 0.6$ and $c_f = 0.1$ [*Van Dongeren et al.*, 2013], which can be explained by Roi-Namur's much smoother topography (Figure 1c) as compared to the Ningaloo reef flat, which remains subaqueous and has relatively high coverage of branching corals.

The validation confirmed the calibrated model settings (Figure 3). The bias and SCI for water levels (row 1), setup (row 2), $H_{rms,IG}$ (row 3), and $H_{rms,inc}$ (row 4) across the reef were small, with some exceptions. On the outer reef flat, the $H_{rms,inc}$ (column c, row 4) was underpredicted and the water levels and setup slightly overpredicted by the model (column c, row 1 and column c, row 2). These deviations suggest that too

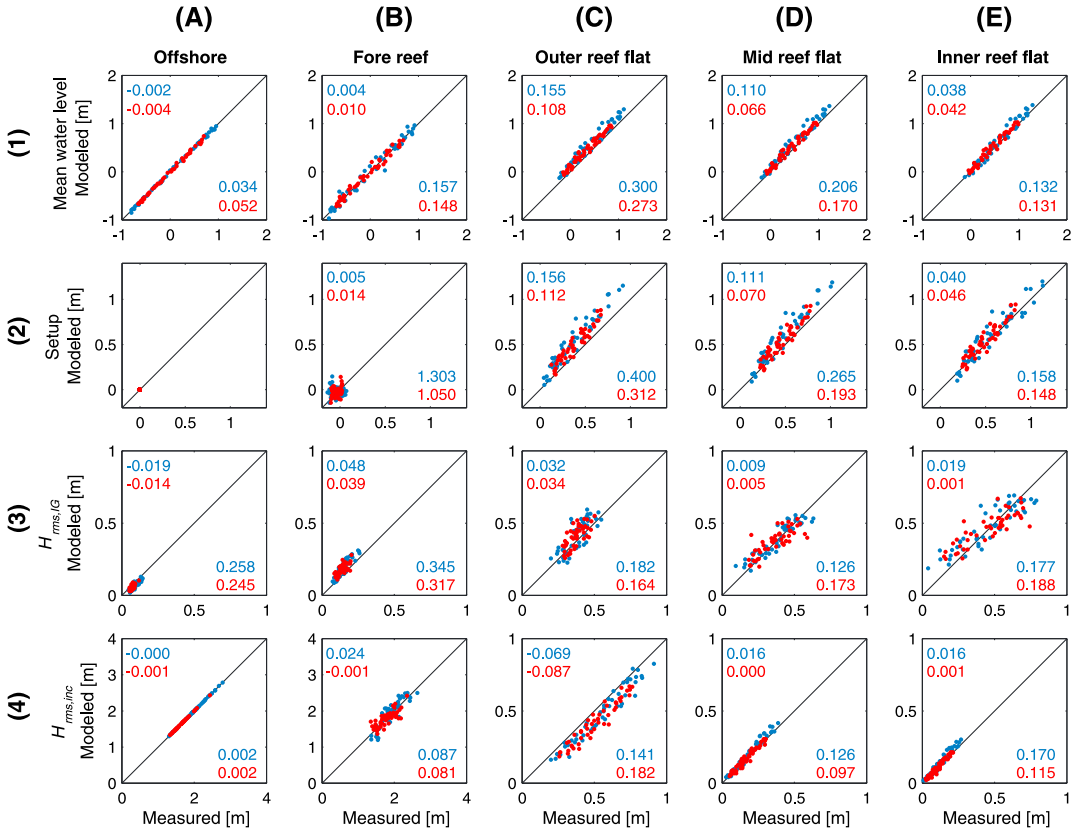

Figure 3. Comparison of measured and modeled burst-averaged mean water level, wave-induced setup, infragravity wave height ($H_{rms,IG}$), and incident wave height ($H_{rms,inc}$) for each instrument. Best model results for calibration (blue) and validation (red) for the following: $f_w = 0.3$, $c_{f,\text{fore reef}} = 0.1$, and $c_{f,\text{reef flat}} = 0.01$. Predictive model skill calculated with bias (top left corner) and scatter index (SCI) (bottom right corner).

much wave-induced setup was generated because the computed waves dissipated too rapidly on the fore reef. A sensitivity analysis (Figures S1 and S2 in the supporting information) revealed that the modeled properties were somewhat sensitive to a variation of the *Roelvink* [1993] wave breaking parameter γ over the range 0.45–0.65 but that optimal results are obtained with the default setting of $\gamma = 0.55$. On this basis and because no wave height observations were taken in the surf zone between the fore reef and outer reef flat, we selected the default value for the predictive model.

4. Effects of Reef Characteristics on Nearshore Hydrodynamics

4.1. Methods

The morphology of a typical atoll or fringing reef is characterized by a steep fore reef slope, relatively wide reef flat, and hydrodynamically rough bathymetry. Due to their variation in coral species, geology, and hydrodynamic conditions, the magnitudes of these characteristics vary widely (Table 1). The Roi-Namur reef characteristics fall within the range where studies have been carried out, and therefore, the model was used to assess the impact of varying reef dimensions, bathymetry, hydrodynamic roughness, and wave and tidal conditions on the resulting nearshore hydrodynamics. We used the model results to identify key parameters controlling wave-driven runup and, thus, flooding of reef-lined coastlines.

The Roi-Namur reef model settings derived in section 3 were used as a base case in the variation simulations. A JONSWAP spectrum was generated from the highest measured waves at Roi-Namur during the March event ($H_{m0} = 3.9$ m; $T_p = 14$ s; Figure 2) and was applied to the offshore model boundary. A sensitivity analysis (not shown) revealed that for this type of reef the hydrodynamics were insensitive to the small undulations in the measured bathymetry. Hence, we characterize the reef geomorphology with a constant-slope fore reef of 1:16, a horizontal reef flat, and a constant beach slope of 1:6. For each

Table 1. Reef Parameter Values and Ranges as Cited in Literature

		Reef Dimensions		Hydrodynamics	
Location	References	Fore Reef Slope (−)	Reef Flat Width (m)	Reef Water Depth (m)	Offshore H_{m0} (m)
Ningaloo, Australia	*Pomeroy et al.* [2012]	1/20	1000	1.00–2.00	0.5–2.8
Lady Elliot Island, Australia	*Jago et al.* [2007]; *Huang et al.* [2012]	–	50–400	0.80–1.70	1.0–3.0
Mururoa, French Polynesia	*Tartinville and Rancher* [2000]	–	100	0.60	1.5–4.0
Ipan, Guam	*Péquignet et al.* [2009]	1/16	400	0.10–1.10	0.5–2.6
Hanalei, Hawaii	*Hoeke et al.* [2013a]	1/18	300	1.00–1.40	3.0–6.0
Molokai, Hawaii	*Storlazzi et al.* [2004]	1/18	500–1000	0.30–2.00	1.0–3.0
Male, Maldives	*Jensen* [1991]	1/1–1/5	140	1.30–3.80	3.0
Majuro, RMI	*Becker et al.* [2014]	1/7	250	0.80–1.00	0.4–1.7
Kwajalein, RMI	*Quataert et al.* [2015] (present study)	1/20	250	0.00–1.00	0.5–3.9
Alphonse, Seychelles	*Hagan and Spencer* [2008]; *Hamylton* [2011]	1/10–1/20	400–500	0.00–0.20	–
	Maximum value	1/1	1000	3.80	6.0
	Minimum value	1/20	50	0.00	0.5

simulation, only one parameter of the base case was varied: fore reef slope, reef flat width, bed friction (hydrodynamic roughness), offshore wave height, and reef flat water depth; the variation of these parameters was based on the ranges listed in Table 1. Each of the 57 simulations (10 permutations for each of the 6 parameters) was run for one cosine-shaped tidal cycle of 12 h with an amplitude of 1 m (a semidiurnal microtidal condition that characterizes most low-latitude tropical coastlines). We use this variation in the offshore mean water level to assess the effect of not only tides but also storm surge and potential sea level rise on the nearshore hydrodynamics (see section 5). Wave height and period were covaried to maintain constant wave steepness; this is consistent with the observations that showed little variation over a range of conditions (mean ± 1 standard deviation of 0.008 ± 0.004).

Model results were postprocessed to derive hourly averaged water levels, wave-induced setup, $H_{rms,inc}$, and $H_{rms,IG}$ at the toe of the beach (cross-shore distance −90 m in Figure 1d). Since the model was not validated for wave runup, due to a lack of a time series of quantitative measurements, we did not use modeled wave runup directly. The $z_{2\%}$ wave runup (wave runup level exceeded by 2% of incident waves) were calculated from the modeled hydrodynamics (water level, $H_{rms,inc}$, $H_{rms,IG}$) at the toe of the beach to obtain a composite quantity that is an indicator for coastal flooding. We used the empirical wave runup method by *Van Gent* [2001] that was originally designed for breakwaters with shallow foreshores and takes into account the combined effects of incident and infragravity waves ($\sqrt{H_{rms,SW}{}^2 + H_{rms,IG}{}^2}$).

4.2. Results

The model runs (Figure 4) show that, generally, wave runup increases with narrower reef flats (column a, row 5), steeper fore reef slopes (column b, row 5), and lower friction on the reef flat (column c, row 5 and column e, row 5) but higher friction on the fore reef slope (column d, row 5). The wave runup also increases with higher offshore water levels (hot colors) and more energetic waves (column f, row 5).

In more detail, variations in the reef flat width (Figure 4, column a) do not affect nearshore mean water levels, as the wave-induced setup is generated on the fore reef and is constant on the reef flat itself in the absence of local radiation stress forcing. Only for very narrow reef flats is a decrease in the water level noticeable. Note that setup is inversely proportional to offshore water level, because the radiation stress exerted by the waves is balanced by the pressure gradient $gh\left(\frac{\delta\eta}{\delta x}\right)$, which for shallower depths leads to larger gradients. For narrower reef flats, $H_{rms,IG}$ and $H_{rms,inc}$ increase which suggests reef flat width affects frictional dissipation rates across the reef.

As the fore reef slope increases (Figure 4, column b), mean water levels increase due to increasing setup. Steeper fore reefs induce a higher pressure response in the cross-shore momentum balance as waves break in a more confined shallower area which results in a larger setup. For fore reef slopes steeper than 1:3, however, the setup decreases again. A momentum balance analysis (not shown) indicates this is the result of a decrease in magnitude of the bed stress term due to the steeper and, thus, deeper

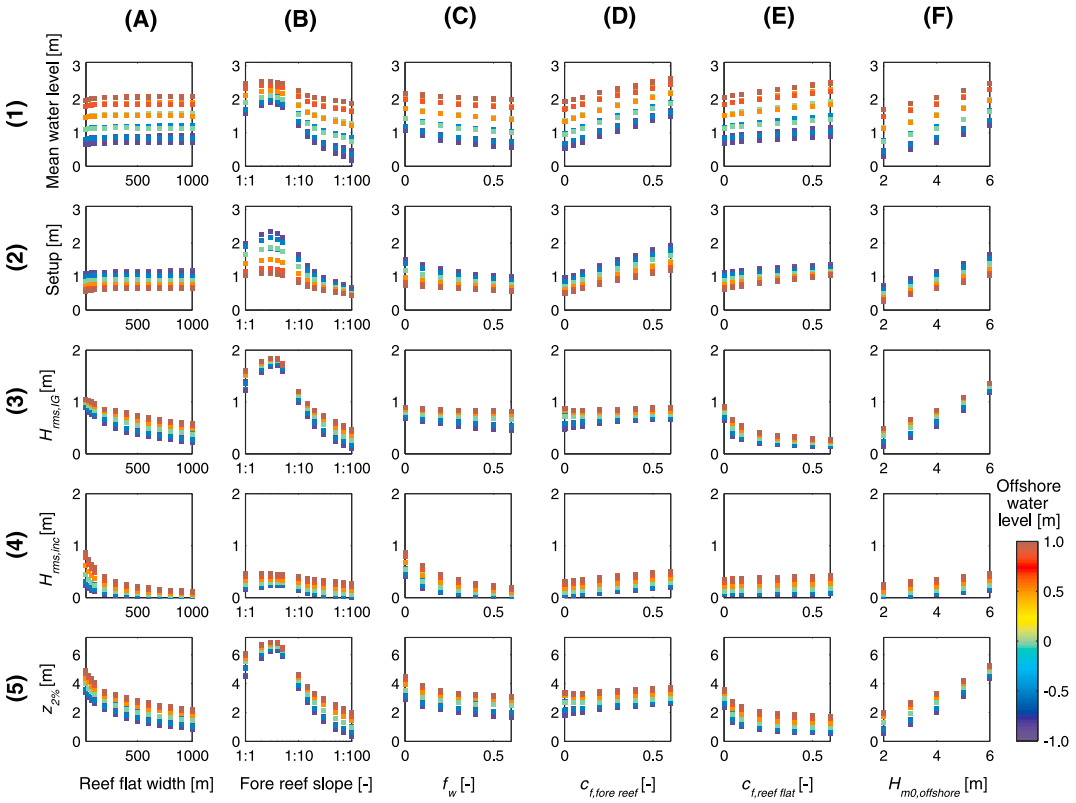

Figure 4. Response of nearshore hydrodynamics (rows 1–5) to variations in reef characteristics (columns a–f) for hourly varying offshore water levels (colors). Wave runup is greatest for very narrow reefs with steep fore reef slopes and deep, smooth reef flats with low coral coverage. Higher water levels, higher waves, and lower bed roughness—all expected effects of climate change—will therefore result in greater wave runup and, thus, coastal flooding.

fore reef slope. In addition, the effect of the offshore water level on the setup variability increases as the fore reef slope increases. $H_{\mathrm{rms,IG}}$ is strongly dependent upon the fore reef steepness, as it controls the infragravity wave generation through the breakpoint mechanism [*Symonds et al.*, 1982; *Pomeroy et al.*, 2012]. $H_{\mathrm{rms,inc}}$ is not dependent on the fore reef slope, as these waves are saturated. A steeper fore reef slope results in increased setup and larger $H_{\mathrm{rms,IG}}$, and this in turn leads to a large increase in wave runup.

A smaller wave friction coefficient (f_w, Figure 4, column c) not only results in larger $H_{\mathrm{rms,inc}}$ but also increases setup on the reef flat. As frictional dissipation decreases, more wave energy is dissipated by wave breaking in shallower water, which results in higher radiation stress gradients and thus more setup. Varying f_w produces no large changes in $H_{\mathrm{rms,IG}}$. The combined effect of increased mean water level and $H_{\mathrm{rms,inc}}$ results in higher wave runup for smaller f_w.

The infragravity and current friction coefficient, c_f (Figure 4, columns d and e), controls $H_{\mathrm{rms,IG}}$ and mean water levels by influencing the bed shear stress term. Higher $c_{f,\mathrm{fore\ reef}}$ (column d) leads to an increase in the bed shear stress, which is balanced by a larger pressure gradient [*Svendsen*, 2003], resulting in higher wave setup and water levels. The $c_{f,\mathrm{fore\ reef}}$ variability has a more pronounced effect on $H_{\mathrm{rms,IG}}$ for lower offshore water levels and $H_{\mathrm{rms,inc}}$, because shallower water levels on the reef flat lead to higher friction dissipation rates. Changes in $c_{f,\mathrm{fore\ reef}}$ have a slight effect on wave runup for lower offshore water levels, due to the subsequent response in reef flat water levels.

An increase in the infragravity and current friction coefficient on the reef flat, $c_{f,\mathrm{reef\ flat}}$, (Figure 4, column e) is balanced by a larger pressure gradient, which in turn drives higher water levels and larger setup. A greater $c_{f,\mathrm{reef\ flat}}$ leads to smaller $H_{\mathrm{rms,IG}}$ due to the increased frictional dissipation. $H_{\mathrm{rms,inc}}$ increases slightly with the increased water depths, but wave runup only increases at very small $c_{f,\mathrm{reef\ flat}}$ values. Together, the results of varying the three bottom friction coefficients demonstrate that bottom roughness affects

wave-induced setup, $H_{rms,inc}$, and $H_{rms,IG}$. A smoother reef flat results in larger $H_{rms,inc}$ and $H_{rms,IG}$ near the shoreline and, therefore, also increases wave runup.

Forcing the model with higher offshore waves, $H_{m0,offshore}$, (Figure 4, column f) results in more wave-induced setup due to increasing radiation stress gradients. The mean water levels, wave heights at the shoreline, and the wave runup increase more or less linearly with increasing $H_{m0,offshore}$ depending on the offshore water level, which is consistent with previous observations [*Merrifield et al.*, 2014; *Péquignet et al.*, 2014].

5. Discussion and Conclusions

The results from this study suggest that important parameters that govern nearshore hydrodynamics on atolls and fringing reefs are the following: reef flat width, fore reef slope, (reef flat) bottom roughness, water levels, and offshore wave conditions. The results demonstrate that under present conditions, coasts fronted by relatively narrow reefs with steep fore reef slopes (~1:10 or steeper) and deeper, smoother reef flats are expected to experience the highest wave runup. Wave runup and, by extension, coastal hazards are likely to increase in the future with predicted climate change.

Coral bleaching events, which are likely to become more frequent due to global climate change [*Hoegh-Guldberg*, 1999], have been shown to kill off corals and result in a decrease in hydrodynamic roughness of coral reefs [*Sheppard et al.*, 2005]. Similarly, ocean acidification may cause reductions in coral cover [*Pandolfi et al.*, 2011] and, thus, hydrodynamic roughness. Together or independently, these processes will reduce bottom friction (f_w, c_f), which would increase wave heights, wave runup, and wave-driven flooding (Figure 4, columns c, d, and e).

According to recent observations [*Vermeer and Rahmstorf*, 2009] and estimates [*Grinsted et al.*, 2009] that include rise due to thermal expansion and ice melting, sea level rise is projected to exceed year 2000 levels by up to 2 m by the end of the 21st century. Because vertical reef flat accretion rates for the coral reefs upon which many carbonate islands sit (1–4 mm/yr; *Montaggioni* [2005]) are up to an order of magnitude smaller than the rates of projected sea level rise (8–16 mm/yr; *Grinsted et al.* [2009]), projected sea level rise will outstrip new reef flat accretion. Taking the modeled tidal variations as sea level variations, this will result in a net increase in water depth over reef flats, which in turn will result in larger wave heights and wave runup (Figure 4). Lastly, new projections [*Storlazzi et al.*, 2015] suggest that climate change will drive changes in extreme wave heights and their directions, which would further alter the resulting nearshore wave heights, water levels, and wave runup (Figure 4, column f).

The results presented here provide coastal managers an estimate of the effect of different coral reef characteristics on potential coastal hazards caused by wave-driven flooding and how these may change in the future. Based on Figure 4, one can determine how a given reef of interest, as defined by its morphology, coral coverage, and oceanographic forcing, may be affected by climate change so as to better constrain future coastal hazards. For example, given the reef geometry of Roi-Namur, it is expected that a combination of lower f_w and higher offshore water levels (Figure 4, column c, row 5) will result in a 200% increase in wave runup. These results, which in the future need to be refined and extended with more data and simulations, provides a first indication of which coastlines may be more susceptible to the effects of climate change. Because climate change will negatively impact corals, efforts to guide coral reef adaptation and/or restoration will be necessary to curtail the likely increased future coastal hazards many tropical shorelines will face.

Acknowledgments
This work was funded by the U.S. Department of Defense's Strategic Environmental Research and Development Program under Project RC-2334 ("The Impact of Sea-Level Rise and Climate Change on Department of Defense Installations on Atolls in the Pacific Ocean"), the U.S. Geological Survey's Pacific Coastal and Marine Science Center, and Deltares through the Deltares Strategic Research in the "Event-driven hydro- and morphodynamics" program (1220002). Joshua Logan, Kurt Rosenberger, and Thomas Reiss (USGS) provided invaluable field and data support. We would like to thank the U.S. Army Garrison-Kwajalein Atoll (USAG-KA) for their overarching support of this project. Use of trademark names does not imply USGS endorsement of products. The USGS data sets presented herein can be obtained by sending a written request to the corresponding author. The XBeach software is available at xbeach.org, and the profile models used can be obtained by sending a written request to Ap van Dongeren (email: Ap.vanDongeren@deltares.nl). The authors would like to thank Steve Monismith and an anonymous reviewer for their helpful feedback.

The Editor thanks two anonymous reviewers for their assistance in evaluating this paper.

References

Becker, J. M., M. A. Merrifield, and M. Ford (2014), Water level effects on breaking wave setup for Pacific Island fringing reefs, *J. Geophys. Res. Oceans*, *119*, 914–932, doi:10.1002/2013JC009373.

Ferrario, F., M. W. Beck, C. D. Storlazzi, F. Micheli, C. C. Shepard, and L. Airoldi (2014), The effectiveness of coral reefs for coastal hazard risk reduction and adaptation, *Nat. Commun.*, *5*, 3794, doi:10.1038/ncomms4794.

Gerritsen, F. (1980), Wave attenuation and wave set-up on a coastal reef, *Proc.17th Int. Conf. Coastal Eng.*, 444–461.

Grady, A. E., L. J. Moore, C. D. Storlazzi, E. Elias, and M. A. Reidenbach (2013), The influence of sea level rise and changes in fringing reef morphology on gradients in alongshore sediment transport, *Geophys. Res. Lett.*, *40*, 3096–3101, doi:10.1002/grl.50577.

Grinsted, A., J. C. Moore, and S. Jevrejeva (2009), Reconstructing sea level from paleo and projected temperatures 200 to 2100 AD, *Clim. Dyn.*, *34*, 461–472.

Hagan, A. B., and T. Spencer, (2008), Reef resilience and change 1998–2007, Alphonse Atoll, Seychelles, paper presented at the *Proc.11th Int. Coral Reef Symp.*, pp. 388–392, Ft. Lauderdale, Fla.

Hamylton, S. (2011), The use of remote sensing and linear wave theory to model local wave energy around Alphonse Atoll, Seychelles, *Estuarine Coastal Shelf Sci.*, *95*(4), 349–358, doi:10.1016/j.ecss.2011.08.035.
Hoegh-Guldberg, O. (1999), Climate change, coral bleaching and the future of the world's coral reefs, paper presented at the *Mar. Fresh Res. 50*, pp. 839–866.
Hoeke, R. K., C. D. Storlazzi, and P. V. Ridd (2013a), Drivers of circulation in a fringing coral reef embayment: A wave-flow coupled numerical modeling study of Hanalei Bay, Hawaii, *Cont. Shelf Res.*, *58*, 79–95, doi:10.1016/j.csr.2013.03.007.
Hoeke, R. K., K. L. McInnes, J. C. Kruger, R. J. McNaught, J. R. Hunter, and S. G. Smithers (2013b), Widespread inundation of Pacific islands triggered by distant-source wind-waves, *Global Planet. Change*, *108*, 128–138, doi:10.1016/j.gloplacha.2013.06.006.
Huang, Z. C., B. Reineman, L. Lenain, W. K. Melville, and J. H. Middleton (2012), Airborne lidar measurements of wave energy dissipation in a coral reef lagoon system, *J. Geophys. Res.*, *117*, C03016, doi:10.1029/2011JC007203.
Jago, O. K., P. S. Kench, and R. W. Brander, (2007), Field observations of wave-driven water-level gradients across a coral reef flat, *J. Geophys. Res.*, *112*, C06027, doi:10.1029/2006JC003740.
Jensen, O. J. (1991), Waves on coral reefs, paper presented at the *Proc. 7th Symp. Coastal and Ocean Management - Coastal Zone*, vol. 91, pp. 2668–2680, Long Beach, AXE, New York.
Lee, T. T., and K. P. Black, (1978), The energy spectra of surf waves on a coral reef, paper presented at the *Proc.16th Int. Conf. Coastal Eng.*, pp. 588–608, ASCE.
Lowe, R. J., J. L. Falter, M. D. Bandet, G. Pawlak, M. J. Atkinson, S. G. Monismith, and J. R. Koseff (2005), Spectral wave dissipation over a barrier reef, *J. Geophys. Res.*, *110*, C04001, doi:10.1029/2004JC002711.
Merrifield, M. A., J. M. Becker, M. Ford, and Y. Yao (2014), Observations and estimates of wave-driven water level extremes at the Marshall Islands, *Geophys. Res. Lett.*, *41*, 7245–7253, doi:10.1002/2014GL061005.
Monismith, S. G., L. M. Herdman, S. Ahmerkamp, and J. L. Hench (2013), Wave transformation and wave-driven flow across a steep coral reef, *J. Phys. Oceanogr.*, *43*, 1356–1379.
Montaggioni, L. F. (2005), History of Indo-Pacific coral reef systems since the last glaciation: Development patterns and controlling factors, *Earth Sci. Rev.*, *71*, 1–75.
Pandolfi, J. M., S. R. Connolly, D. J. Marshall, and A. L. Cohen (2011), Projecting coral reef futures under global warming and ocean acidification, *Science*, *333*(6041), 418–422, doi:10.1126/science.1204794.
Péquignet, A. C., J. M. Becker, M. A. Merrifield, and J. Aucan (2009), Forcing of resonant modes on a fringing reef during tropical storm Man-Yi, *Geophys. Res. Lett.*, *36*, L03607, doi:10.1029/2008GL036259.
Péquignet, A.-C. N., J. M. Becker, and M. A. Merrifield (2014), Energy transfer between wind waves and low-frequency oscillations on a fringing reef, Ipan, Guam, *J. Geophys. Res. Oceans*, *119*, 6709–6724.
Pomeroy, A., R. J. Lowe, G. Symonds, A. R. Van Dongeren, and C. Moore (2012), The dynamics of infragravity wave transformation over a fringing reef, *J. Geophys. Res.*, *117*, C11022, doi:10.1029/2012JC008310.
Roelvink, J. A. (1993), Dissipation in random wave groups incident on a beach, *Coastal Eng.*, *19*, 127–150.
Roelvink, J. A., A. Reniers, A. R. van Dongeren, J. van Thiel de Vries, R. McCall, and J. Lescinski (2009), Modelling storm impacts on beaches, dunes and barrier islands, *Coastal Eng.*, *56*(11–12), 1133–1152, doi:10.1016/j.coastaleng.2009.08.006.
Sheppard, C., D. J. Dixon, M. Gourlay, A. Sheppard, and R. Payet (2005), Coral mortality increases wave energy reaching shores protected by reef flats: Examples from the Seychelles, *Estuarine Coastal Shelf Sci.*, *64*(2–3), 223–234, doi:10.1016/j.ecss.2005.02.016.
Storlazzi, C. D., A. S. Ogston, M. H. Bothner, M. E. Field, and M. K. Presto (2004), Wave- and tidally-driven flow and sediment flux across a fringing coral reef: Southern Molokai, Hawaii, *Cont. Shelf Res.*, *24*(12), 1397–1419, doi:10.1016/j.csr.2004.02.010.
Storlazzi, C. D., E. Elias, M. E. Field, and M. K. Presto (2011), Numerical modeling of the impact of sea-level rise on fringing coral reef hydrodynamics and sediment transport, *Coral Reefs*, *30*(S1), 83–96, doi:10.1007/s00338-011-0723-9.
Storlazzi, C. D., J. B. Shope, L. H. Erikson, C. A. Hegermiller, and P. L. Barnard (2015), Future wave and wind projections for U.S. and U.S.-affiliated pacific islands, U.S. Geological Survey Open-File Report 2015–1001, pp. 426, doi:10.1016/j.csr.2004.02.010.
Svendsen, I. A. (2003), *Introduction to Nearshore Hydrodynamics, Advanced Series on Ocean Engineering: Volume 24*, World Scientific, Singapore.
Symonds, G., D. A. Huntley, and A. J. Bowen (1982), Long wave generation by a time-varying breakpoint, *J. Geophys. Res.*, *87*(C1), 492–498, doi:10.1029/JC087iC01p00492.
Tartinville, B., and J. Rancher (2000), Wave-induced flowover Mururoa Atoll Reef, *J. Coastal Res.*, *16*(3), 776–781.
Van der Westhuysen, A. J. (2010), Modeling of depth-induced wave breaking under finite depth wave growth conditions, *J. Geophys. Res.*, *115*, C01008, doi:10.1029/2009JC005433.
Van Dongeren, A. R., A. J. H. M. Reniers, and J. A. Battjes (2003), Numerical modeling of infragravity wave response during DELILAH, *J. Geophys. Res.*, *108*(C9), 3288, doi:10.1029/2002JC001332.
Van Dongeren, A. R., R. J. Lowe, A. Pomeroy, D. M. Trang, J. A. Roelvink, G. Symonds, and R. Ranasinghe (2013), Numerical modeling of low-frequency wave dynamics over a fringing coral reef, *Coastal Eng.*, *73*, 178–190, doi:10.1016/j.coastaleng.2012.11.004.
Van Gent, M. R. A. (2001), Wave runup on dikes with shallow foreshores, *J. Waterway Port Coastal Ocean Eng.*, *127*(September/October), 254–262.
Vermeer, M., and S. Rahmstorf (2009), Global sea level linked to global temperature, paper presented at the *Proc. Natl. Acad. Sci.*, *106*, pp. 21,527–21,532.
Vetter, O., J. M. Becker, and M. A. Merrifield (2010), Wave setup over a Pacific Island fringing reef, *J. Geophys. Res.*, *115*, C12066, doi:10.1029/2010JC006455.
Young, I. R. (1989), Wave transformation over coral reefs, *J. Geophys. Res.*, *94*(C7), 9779–9789, doi:10.1029/JC094iC07p09779.